JAST, Vol. 3, No. 4, pp 205–212

JAST
Journal of Aerospace Science and Technology

On the Dependence of Soot Formation and Combustion on Swirling Combustion Furnaces: Measurement and Simulation

K. Bashirnezhad[1], M. Moghiman[2], M. Mousavi[3]

Soot concentration distribution is investigated both numerically and experimentally in methane-air diffusion flame. The experimental work is conducted with a cylindrical swirl stabilized combustor. Filter paper technique is used to measure soot volume fraction inside the combustor. The numerical simulation is based on the solution of the fully-coupled conservation equations for swirling turbulent flow, chemical species kinetic modeling, fuel combustion and soot formation and oxidation. The soot particle number density and the mass density based on the acetylene concentrations are used to model the soot emission in confined swirling turbulent diffusion flame. The comparison between predictions and measurement results over a range of different swirl numbers shows good agreement. The results reveal the significant influence of swirl intensity on combustion characteristics and soot formation in diffusion flames. An increase in swirl number enhances the mixing rate, peak temperature, and soot volume fraction inside the flame zone. The locations to give the maximum temperature and soot concentration shift to backward (close to combustor inlet) with increase in swirl number.

NOMENCLATURE

c_1	scaling factor for the soot inception model (s^{-1})
c_2	scaling factor for the soot growth ($kg.m.kmol^{-1}.s^{-1}$)
c_3	scaling factor for the O_2 oxidation rate ($kg.m.kmol^{-1}.k^{0.5}.s^{-1}$)
c_4	scaling factor for the OH oxidation rate ($kg.m.kmol^{-1}.k^{0.5}.s^{-1}$)
D_b	burner throat diameter (m)
h	enthalpy ($j.kg^{-1}$)
G_ϕ	axial flux of angular momentum ($kg.m^2.s^{-2}$)
G_x	axial flux of linear momentum ($kg.m.s^{-2}$)
m	mass fraction
M	soot mass density ($kg.m^{-3}$)
N	soot particle number density(m^{-3})
N_A	Avogadro's number
r	radial direction (m)
R	universal gas constant
R_j	reaction rate mass of the j th species
SN	swirl number
$S_h^\bullet$	energy conservation equation source term
T	mean temperature (k)
u	axial velocity component ($m.s^{-1}$)
v	radial velocity component ($m.s^{-1}$)
w	swirl velocity ($m.s^{-1}$)
W	molecular weight ($kg.kmol^{-1}$)
x	axial direction (m)

Greek letters

μ	molecular viscosity of gas phase ($kg.m^{-1}.s^{-1}$)

1. *PhD Candidate, Dept. of Mechanical Eng., Islamic Azad Univ., Mashhad, Iran, Email: bashirnezhad@yahoo.com.*
2. *Professor, Dept. of Mechanical Eng., Ferdowsi University, Mashhad, Iran.*
3. *Assistant Professor, Dept. of Chemical Eng., Ferdowsi University, Mashhad, Iran.*

ρ gas phase density (kg.m^{-3})
η collision efficiency of soot particles
Γmj Laminar exchange coefficient

INTRODUCTION

The non-premixed flames often contain locally fuel-rich regions where the decomposition products of the fuel react with one another to produce larger hydrocarbons instead of being oxidized to carbon dioxide and water. This process, termed hydrocarbon growth, is normally undesirable since it ultimately produces soot particles and carcinogenic polycyclic aromatic hydrocarbons (PAH) according to Mecnally et al. [1] and Roesler et al. [2]. The process of soot production from hydrocarbon fuels consists of fuel pyrolysis, formation of polycyclic aromatic hydrocarbons, particle inception, coagulation, surface growth, and oxidation [3, 4]. The soot formation is strongly dependent on the PAH concentration and temperature domain [5].

The formation/combustion of soot in laminar and simple turbulent jet diffusion flames has been studied by many researchers [6-10]. Brooks and Moss [9] presented results of numerical modeling of piloted axisymmetric turbulent methane-air simple jet (without swirl) flames using an extended flamelet approach. Kronenburg et al. [10] investigated the modeling of soot formation and oxidation in the same flames by the conditional moment closure (CMC) method. Generally, good agreement with the experiments has been achieved by the two models. Swirling flows are used in many technical applications particularly in furnaces and gas turbines to improve flame stabilization, ignition stability, mixing enhancement, pollutant reduction and blow-off characteristics [11, 12]. Although the effect of many parameters on soot formation has been investigated by many investigators, the influence of swirl intensity on soot formation of methane diffusion flames has not been studied. The aim of this paper is to study the effect of swirl intensity on soot formation and oxidation in swirling turbulent diffusion flames. The investigation is conducted with both numerical simulation and measurements.

EXPERIMENTAL SET-UP

A horizontal laboratory combustor with a circular cross-section designed and constructed to confine the flame and prevent gas composition fluctuations resulting from the ambient air. The combustor is 360 mm in diameter and 1000 mm in length, which ensures simulation of the essential physics of combustor. An air swirler is installed at the front of the burner and the swirl level is easily controlled by varying the swirler. A schematic diagram of the experimental set-up is illustrated in Figure 1.

Some circular slots are cut into the upper side of the combustor body so that the soot meter and thermocouple probes can be inserted into the center of the cylindrical combustor. Soot concentration is measured using the filter paper technique [13]. The temperature inside the combustor is measured using the ceramic-sheathed type S-thermocouples with a thermal resistance up to 2000 K. The described system measures temperatures within a tolerance of 1 K. Mass flow rate of the fuel and air are measured by using a Rota meter with the accuracy of 0.1lit/min. The inlet surface areas of air and fuel streams are 96 and 2 cm^3 respectively. The temperature fluctuation of the inlet air and fuel is kept within the specified margins of 3 K. The repeatability of the data is regularly checked during each experimental session. On average, all of the data can be reproduced to within 10% of the mean value. The combustor flow-gas is continuously monitored during the measurement program to sense any change in the combustor operating conditions. In addition, although every effort is made to eliminate sources of gas leakage in the combustor construction, the combustor pressure is maintained close to atmospheric value.

MATHEMATICAL MODELING

In this study, the following basic assumptions are made to produce a mathematical model for various processes inside the combustor:

1. One considers that an axisymmetric two-dimensional computational fluid dynamics analysis of a turbulent diffusion flame is able to predict gas velocity, temperature, and 14 species concentration profiles with sufficient accuracy.
2. The soot particle phase is considered to be dilute and is considered not to affect the gas flow field.
3. The soot formation model is based of acetylene concentration and soot combustion model is based OH and O_2 concentration.
4. Buoyancy forces are neglected.
5. The dynamic viscosity is independent of temperature.
6. Methane is considered as the fuel.

The mathematical model is based on a typical Eulerian formulation. The time averaged equations are as follows:
Continuity and momentum equations:

$$\frac{\partial u}{\partial x}+\frac{1}{r}\frac{\partial}{\partial r}(rv)=S^{\bullet} \tag{1}$$

$$\frac{1}{r}\left[\frac{\partial}{\partial x}(r\rho uu)+\frac{\partial}{\partial r}(r\rho uv)\right]=-\frac{\partial p}{\partial x} + \mu\nabla^2 u-\frac{1}{r}\frac{\partial}{\partial r}(r\rho\overline{u'v'})-\frac{\partial}{\partial x}(\rho\overline{u'u'}) \tag{2}$$

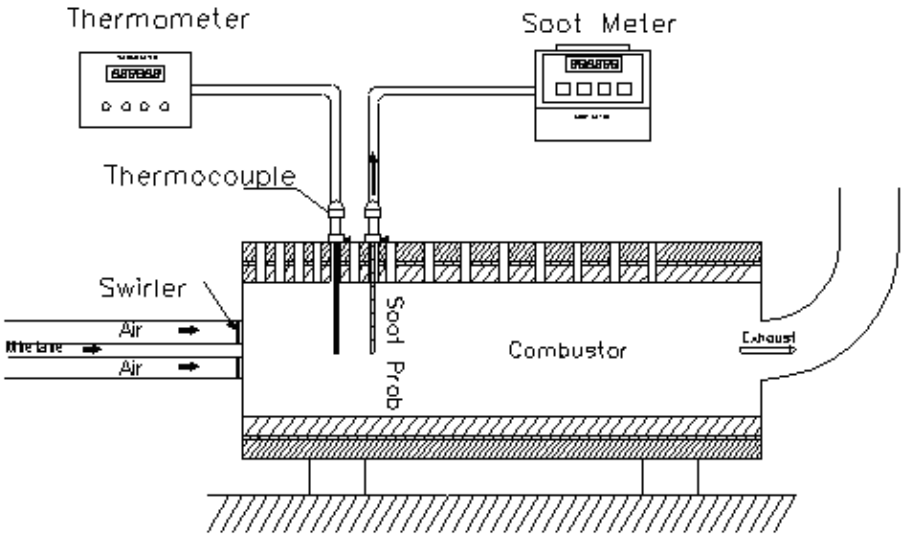

Figure 1. Schematic of the experimental set-up.

$$\frac{1}{r}\left[\frac{\partial}{\partial x}(r\rho uv)+\frac{\partial}{\partial r}(r\rho vv)-\rho w^2\right]= -\frac{\partial p}{\partial r}+\mu(\nabla^2 v+\frac{v}{r^2})-\frac{1}{r}\frac{\partial}{\partial r}(r\rho\overline{v'v'}) -\frac{\partial}{\partial x}(\rho\overline{u'v'})-\frac{1}{r}\rho\overline{w'w'} \quad (3)$$

$$\frac{1}{r}\left[\frac{\partial}{\partial x}(r\rho uw)+\frac{\partial}{\partial r}(r\rho vw)+\rho vw\right]= \mu(\nabla^2 w-\frac{w}{r^2})-\frac{1}{r}\frac{\partial}{\partial r}(r\rho\overline{v'w'}) -\frac{\partial}{\partial x}(\rho\overline{u'w'})-\frac{1}{r}\rho\overline{v'w'} \quad (4)$$

The turbulent stresses are calculated from an algebraic stress model [14]. Furthermore, a conventional wall-function approach is used in the near-wall region to bridge the viscous sublayer. The same boundary conditions as the experiment are applied in this study and are shown in Table 1. The turbulent intensities and eddy length scales are set to the same values on the inlet boundaries of the fuel and air.

The swirl number (SN), which is a non-dimensional parameter, characterizes the degree of swirl in a swirl flow and is defined as the ratio of the axial flux of angular momentum to the axial flux of axial momentum [11 , 14]. At the air inlet of the burner chamber,

$$SN=\frac{2G_\phi}{G_x D_b}=\frac{2\int_0^{D_b/2}\rho uwr^2dr}{D_b\int_0^{D_b/2}\rho u^2 rdr} \quad (5)$$

Table 1. Boundary conditions of the CFD model.

	air			fuel
	inlet	wall	outlet	inlet
u	3	wall-function	$\partial u/\partial x=0$	10
v	0	wall-function	$\partial v/\partial x=0$	0
w	Variable	wall-function	$\partial w/\partial x=0$	0
T	298	$\partial T/\partial r=0$	$\partial T/\partial x=0$	298

Energy equation:

$$\frac{1}{r}\left[\frac{\partial}{\partial x}(r\rho uh)+\frac{\partial}{\partial x}(r\rho vh)\right]=\Gamma_h\nabla^2 h -\frac{1}{r}\frac{\partial}{\partial r}(r\rho\overline{v'h'})-\frac{\partial}{\partial x}(\rho\overline{u'h'})+S_h^\bullet \quad (6)$$

The energy addition due to combustion ($S_h^\bullet$) is determined using a reduced mechanism for methane combustion based on results from Chen [15]. The global steps of this 10-step mechanism and 14 species include CH_4, CH_3, O, O_2, H, H_2, CO, CO_2, OH, C_2H_2, C_2H_4, C_2H_6, H_2O, and CH_2O as summarized below:

$$O_2+2CH_3+C_2H_4=H+2CH_4+CO_2+1/2C_2H_2 \quad (R1)$$

$$O_2+2CH_3=H_2+CH_4+CO_2 \quad (R2)$$

$$O_2+3CH_3=H+2CH_4+CO_2 \quad (R3)$$

$$O_2+CH_3+CO=H+CO_2+CH_2O \quad (R4)$$

$$O_2+CO+C_2H_6=CH_4+CO_2+CH_2O \quad (R5)$$

$$O_2+2CO=2CO_2 \quad (R6)$$

$$H + O_2 + CO = OH + CO_2 \quad (R7)$$

$$H_2 + O_2 + CO = H + OH + CO_2 \quad (R8)$$

$$O_2 + H_2O + CO = 2OH + CO_2 \quad (R9)$$

$$O_2 + 1/2C_2H_2 = H + CO_2 \quad (R10)$$

In this study, the reaction rates that appear as source terms in species transport equations (Eq. (6)) are controlled by an Arrhenius kinetic rate expression. The Arrhenius reaction rate for species α in the k -th reaction ($R_{\alpha,k}$) is calculated from Chen [15], as:

$$R_{\alpha,k} = \left(\nu''_{\alpha,k} - \nu'_{\alpha,k}\right) k_k \prod_{j=1}^{84} (C_j)^{v'_j} \quad (7)$$

where $\nu'_{\alpha,k}$ is the stoichiometric coefficient of reactant α in reaction k, $\nu''_{\alpha,k}$ is the stoichiometric coefficient of product α in reaction k, k_k is the reaction rate coefficient in reaction k and C_j is the molar concentration of each reactant or product species j. The flow field equations are completed by the ideal equation of state, which determines the distribution of density as:

$$\rho = \frac{P}{RT}\left[\sum \frac{m_j}{M_j}\right] \quad (8)$$

This assumption is appropriate since the high temperatures associated with combustion generally result in sufficiently low densities to be ideal gas behavior as a reasonable approximation.

$$\frac{1}{r}\left[\frac{\partial}{\partial x}(r\rho u m_j) + \frac{\partial}{\partial r}(r\rho v m_j)\right] = \Gamma_{mj}\nabla^2 m_j - \frac{1}{r}\frac{\partial}{\partial r}(r\rho\overline{v'm'_j}) - \frac{\partial}{\partial x}(\rho\overline{u'm'_j}) + R_j + S_j \quad (9)$$

Where R_j is the mass rate of reaction or depletion by chemical reactions and Γ_{mj} is the laminar exchange coefficient. In this study, species conservation equation is solved for all of the 14 species.

Soot modeling

The emission of soot from a flame is determined by a competition between soot formation and oxidation, which must be considered when a soot modeling study is carried out. In this study, a recent soot model developed by Brookes et al. [9] is used. The model describes the soot formation in terms of the soot particle number density (N) as well as the soot particle mass density (M), and takes into account the inception (nucleation), coagulation, growth, and oxidation processes for the rates of these two parameters as:

$$\frac{DN}{Dt} = \left(\frac{dN}{dt}\right)_{Inception} + \left(\frac{dN}{dt}\right)_{Coagulation} \quad (10)$$

$$\frac{DM}{Dt} = \left(\frac{dM}{dt}\right)_{Inception} + \left(\frac{dM}{dt}\right)_{Growth} + \left(\frac{dM}{dt}\right)_{Oxidation} \quad (11)$$

The model proposed by Leung et al. [16] is used to predict soot inception. In this model, it is assumed that acetylene is primarily responsible for the nucleation and growth of soot particles. The inception step is treated simply as a one-step process:

$$C_2H_2 \rightarrow 2C_{SOOT} + H_2 \quad (12)$$

The rate of inception is assumed to be first order in acetylene concentration so that the rate is calculated as:

$$\left(\frac{dN}{dt}\right)_{Inception} = c_1 N_A \left(\rho\frac{m_{C_2H_2}}{W_{C_2H_2}}\right) e^{-21100/T} \quad (13)$$

$$\left(\frac{dM}{dt}\right)_{Inception} = \frac{M_P}{N_A}\left(\frac{dN}{dt}\right)_{Inception} \quad (14)$$

where M_p, the mass of a soot nucleus, has a value of 144 kg.kmol^{-1} based on the assumption that the soot size corresponds to 12 carbon atoms and c_1=54 s^{-1} is determined by Brookes and Moss [9]. Assuming the particles are mono-dispersed in size and spherical, the coagulation rate and reaction surface or growth rate are given by:

$$\left(\frac{dN}{dt}\right)_{coagulation} = -\left(\frac{24R}{\rho_{Soot}N_A}\right)^{1/2} \times \left(\frac{6}{\pi\rho_{Soot}}\right)^{1/6} T^{1/2} M^{1/6} N^{11/6} \quad (15)$$

$$\left(\frac{dM}{dt}\right)_{growth} = c_2\left(\rho\frac{m_{C_2H_2}}{W_{C_2H_2}}\right) e^{-21100/T} \times \left((\pi N)^{1/3}\left(\frac{6M}{\rho_{Soot}}\right)^{2/3}\right) \quad (16)$$

where ρ_{soot} = 2000 kg.m^{-3} and c_2 =9000.6 kg·m·kmol^{-1} ·s^{-1} according to Brookes et al. [9]. The oxidation model takes into account combustion of soot by O_2 and OH radicals. In this model, the rate of soot oxidation is given by:

$$\left(\frac{dM}{dt}\right)_{Oxidation} = -c_4\rho\eta\frac{m_{OH}}{W_{OH}}\sqrt{T}(\pi N)^{1/3}\left(\frac{6M}{\rho_S}\right)^{2/3} \times - c_3\rho\frac{m_{O_2}}{W_{O_2}}Exp(\frac{-19778}{T})\sqrt{T}\,(\pi N)^{1/3}\left(\frac{6M}{\rho_{Soot}}\right)^{2/3} \quad (17)$$

where η is set to be 0.13, c_3=8 9 0 3 ,5 1 kg·m·kmol^{-1}·K$^{1/2}$ and c_4=105.81 kg·m·kmol^{-1} ·K$^{-1/2}$·s^{-1}, which are obtained by converting the rate of soot mass consumption [9].

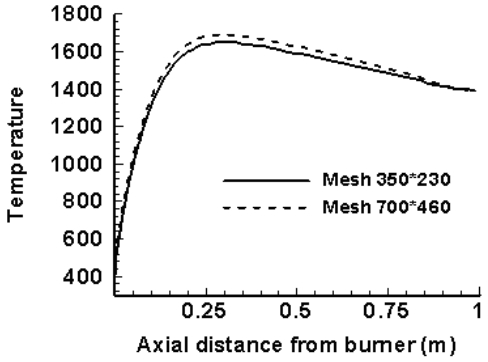

Figure 2. Effect of mesh numbers on centerline temperature.

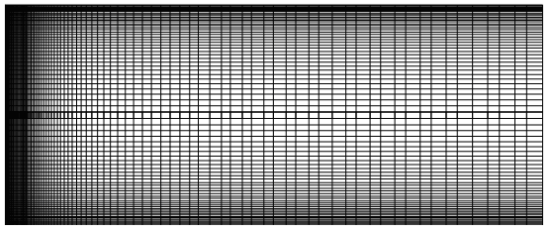

Figure 3. The computational grid.

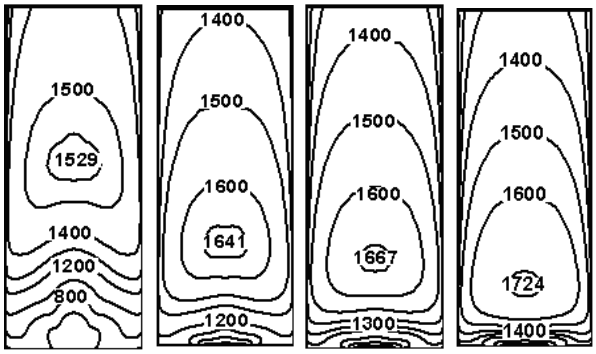

(a) SN=0.0 (b) SN=0.2 (c) SN=0.4 (d) SN=0.6

Figure 4. Effect of swirl number on predicted temperature contours.

METHOD OF SOLUTION

An in-house CFD code is used to calculate the mass, momentum, and energy equations as well as model turbulent flow, fuel combustion, and soot formation. The conservation equations are solved using a control-volume based computational procedure [17]. The convective terms are discretized by the power law scheme. The flow field pressure linked equations are solved by the SIMPLE algorithm and the set of algebraic equations are solved sequentially with the line-by-line method which is a combination of Gauss-Seidel method and tridiagonal-matrix algorithm. The convergence criterion is determined by the requirement that the maximum value of the normalized residuals of any equation must be less than 1×10^{-5}. Under-relaxation factor is chosen as 0.25 for all dependent variables. A numerical mesh of 350 $\times$ 230 grid nodes is used after several calculations because further refinement in either direction does not change the result (maximum difference in velocity, temperature, and other scalar functions in the carrier phase) by more than 2% as shown in Figure 2 for centerline temperature in two different meshes. The grid spacing in axial and radial directions are changed smoothly (see Figure 3) to minimize the deterioration of the formal accuracy of the discretization scheme due to variable grid spacing and in such a way that higher concentration of nodes occur near the inlet and the walls.

Because of the elliptic nature of the conservation equations, boundary conditions are specified at all boundaries of the domain considered. The air enters the combustor with the temperatures of 298 K and the axial velocity of 3 m/s while different swirl numbers are investigated. Mass flow-rates of the gas fuel and air, are injected at 298 K, equal to 0.1 and 1.72 kg/min. Furthermore, a zero axial gradient is prescribed for all variables at the outlet.

RESULTS AND DISCUSSION

Figure 4 shows the simulated contours of temperature inside the combustor for different swirl numbers. The results show that an increase in swirl number raises the combustor peak temperature. This occurs because an increased swirl number increases combustion efficiency due to enhancement of mixing rates between the fuel and the oxidant. The location to give the maximum temperature shifts forward with a decrease in swirl number. This shift corresponds to the fact that the combustion zone of the diffusion flame is enlarged with a decrease in swirl number. This observation is in accord with the results of Yapici et al. [18].

Comparison between the computed and measured temperatures is shown in Figure 5. It can be seen that the predicted temperature profiles have very good agreement with measurement results, especially with respect to the maximum temperature value and its location. The results show that the 10 steps reduced mechanism used as combustion model is able to predict methane-air diffusion flame characterizations with sufficient accuracy [15]. There are some deviations between the measurement and prediction temperatures. This occurs because the soot radiation effect is not included in the numerical prediction.

Measured and computed soot volume fractions are compared in Figure 6, where the centerline soot volume fraction profiles are plotted for different swirl numbers. It is observed that the agreements between measured and predicted results are satisfactory. There is a slight discrepancy between the predictions and measurements for condition SN=0.0. This occurs because the advanced algebraic stress model used in

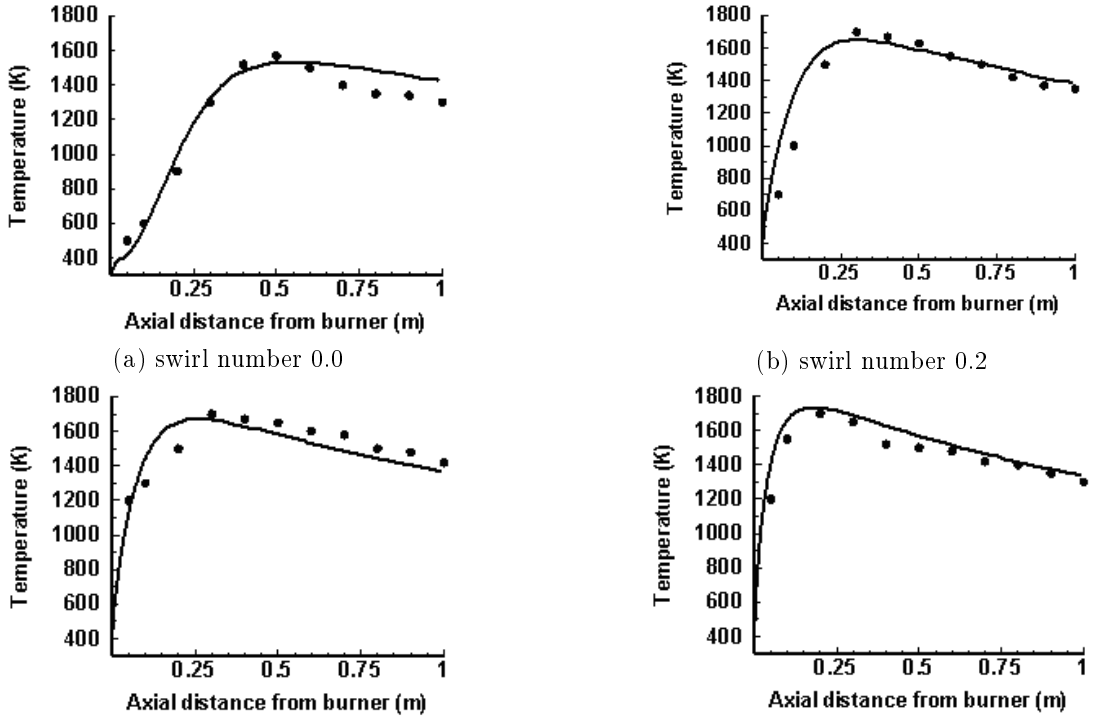

(a) swirl number 0.0 (b) swirl number 0.2

(c) swirl number 0.4 (d) swirl number 0.6

Figure 5. Comparison between the computed (lines) and measured (symbols) centerline temperatures for different swirl numbers.

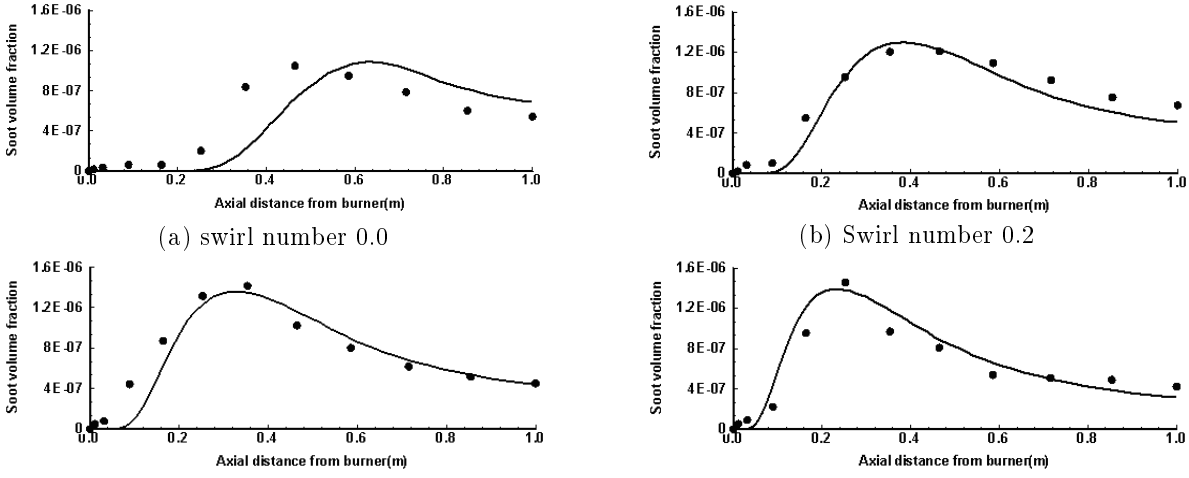

(a) swirl number 0.0 (b) Swirl number 0.2

(c) Swirl number 0.4 (d) Swirl number 0.6

Figure 6. Comparison between the computed (lines) and measured (symbols) centerline soot volume fractions for different swirl numbers.

this study has been developed for predicting highly swirling flows [14]. Measurements show higher soot volume fraction in the vicinity of the point of the issue.

Considering the soot model equations specify two main parameters that affect soot formation, i.e. acetylene concentration and soot particle density which need to be analyzed more. Figure 7 shows centerline acetylene concentrations for three swirl numbers 0.2, 0.4, and 0.6. Acetylene concentration plays an effective role in soot nucleation and surface growth [10,16]. It can be seen that as expected, the location of peak C_2H_2 mass fraction is in the vicinity of the combustor inlet zone, where the fuel concentration and temperature levels are high (see Figures 4 and 5). The figure shows

that swirl intensity can affect peak value of acetylene concentration and its location in combustor. It is seen that an enhancement in swirl number increases C_2H_2 peak concentration.

Figure 8 displays the centerline distributions of soot particles density for three swirl numbers. It can be seen that soot particles density along the combustor centerline increases to a maximum and then decreases. As expected, the trend of variation of soot particles density is similar to the variation of temperature profiles (see Figure 5). The distribution of the soot number density moves towards the combustor inlet with an increase in swirl number.

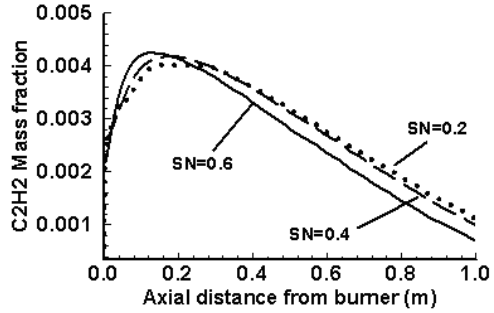

Figure 7. Effect of swirl number on predicted centerline acetylene concentrations.

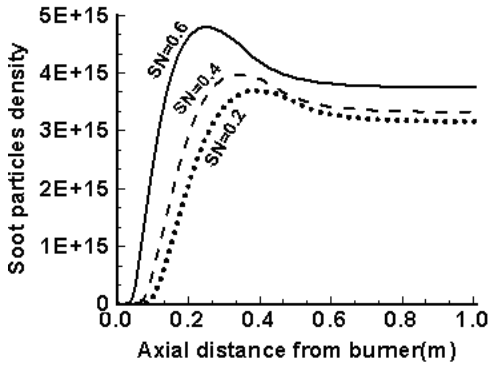

Figure 8. Effect of swirl number on predicted centerline soot particles density.

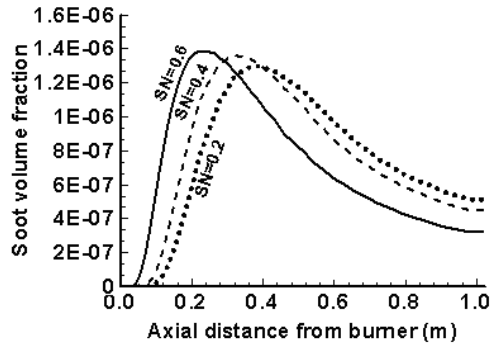

Figure 9. Effect of swirl number on predicted centerline soot volume fractions.

Figure 9 presents the influence of swirl number on soot volume fractions along the combustor centerline. It can be seen that swirl intensity affects the peak soot concentration and its location. Clearly the distribution of soot volume fraction along the combustor centerline strongly depends on the distribution of temperature and acetylene mass fraction (see Figures 4 and 7).

CONCLUSION

Burning behaviors of non premixed methane-air flame are experimentally and computationally studied for different swirl numbers. The soot particle number density and the mass density based on the acetylene concentrations are used to model the soot emission in confined swirling turbulent diffusion flames. The results show the significant influence of swirl number on soot distribution inside the combustor. The results also show that an increase in swirl number enhances the mixing rate, peak temperature, and peak soot volume fraction near the burner. Moreover, they reveal that although peak soot concentration is initially increased with increasing swirl number, owing to the increase of mixing rate and soot oxidation, soot emission from the furnace is decreased. The comparison shows a good agreement between the numerical predicted results and the measurements.

REFERENCES

1. Mcenally C. S., Ciuparu D. M.and Pfefferle L. D., "Experimental Study of Fuel Decomposition and Hydrocarbon Growth Processes for Practical Fuel Components: Heptanes", *J. of Combustion and Flame*, **134**, PP 339-353(2003).
2. Roesler J. F., Martinot S., Mcenally C. S., Pfefferle L. D., Delfau J. L. and Vovelle C., "Investigating the Role of Methane on the Growth of Aromatic Hydrocarbons and Soot in Fundamental Combustion Processes", *J. of Combustion and Flame*, **134**, PP 249-260(2003).
3. Yang B. and Koylu U.O., "Detailed Soot Field in a Turbulent Non-Premixed Ethylene/air Flame from Laser Scattering and Extinction Experiments", *J. of Combustion and Flame*, **141**, PP 55-65(2005).
4. Gruenberger T.M., Moghiman M., Bowen P.J. and Syred N., "Dynamic of Soot Formation by Turbulent Combustion and Thermal Decomposition of Natural gas", *J. of Combustion Science and Technology*, **174**, PP 67-86(2002).
5. Frenklach M., "Reaction Mechanism of Soot Formation in Flames", *J. of Physical Chemistry Chemical Physics*, **4**, PP 2028-2037(2002).
6. Skjth-Rasmussen M.S., Glarborg P., ?stberg M., Johannessen J. T., Livbjerg H., Jensen A. D. and Christensen T. S., "Formation of Polycyclic Aromatic Hydrocarbons and Soot in Fuel-Rich Oxidation of Methane in a Laminar Flow Reactor", *J. of Combustion and Flame*, **136**, PP 91-128 (2004).

7. Broookes S. J. and Moss J. B., "Measurements of Soot Production and Thermal Radiation From Confined Turbulent Jet Diffusion Flames of Methane", *J. of Combustion and Flame*, **116**, PP 49-16(1999).

8. Beltrame A., Porshnev P., Merchan M. W., Saveliev A., Fridman A., Kennedy L. A., Petrova O., Zhdnok S., Amouri F., and Charon O., "Soot and NO Formation in Methane-Oxygen Enriched Diffusion Flames", *J. of Combustion and Flame*, **124**, PP 295-310(2001).

9. Brookes S.J. and Moss J.B., "Predictions of Soot Thermal Radiation Properties in Confined Turbulent Jet Diffusion Flames", *J. of Combustion and Flame*, **116**, PP 486-503(1999).

10. Kroneburg A., Bilger R. W., and KENT J. H., "Modeling Soot Formation in Turbulent Methane-Air Jet Diffusion Flame", *J. of Combustion and Flame*, **121**, PP 24-40(2000).

11. Moghiman M. and Maneshkarimi M. R., "Effect of Swirl Number and Droplet Size on Turbulent Spray Combustion", *J. of Iranian Mechanical Engineering*, **5**, PP 47-59(2000).

12. Aoki H., Furuhata T., Tanno S., Miura T., and Ohtani S., "Effect of Swirling Flow on Unburned Ratio and Nitrogen Oxide Concentration in a Spray Combustion System", *J. of Experimental Thermal and Fluid Science*, **5**, PP 838-847(1992).

13. AVL, "Smoke Measurement", *AVL LIST GMBH*, Graz, (2001).

14. Zhang J., Nieh S., and Zhou L., "A New Version of Algebraic Stress Model for Simulating Strongly Swirling Flows", *J. of Numerical Heat Transfer* , **22**, PP 49-62(1992).

15. Chen, J.Y., "Workshop on Numerical Aspects of Reduction in Chemical Kinetics", CERMICS-ENPC, Cite Descartes, Champus sur Marne, France, (1997).

16. Lueng K.M, Lindstedt R.P., and Jones W.P., "A Simplified Reaction Mechanism for Soot Formation in Nonpremixed Flames", *J. of Combustion and Flame*, **87**, PP 289-305(1997).

17. Versteeg H. K. and Malalaseke W., "An Introduction to Computational Fluid Dynamics-The Finite Volume Method", Longman, (1984).

18. Yapici H., Kayatas N., Albayrak B., and Basturk G., "Numerical Calculation of Local Entropy Generation in a Methane-Air Burner", *J. of Energy Conversion and Management*, **46**, PP 1885-1919(2005).